

Article

Effects of River Discharge and Sediment Load on Sediment Plume Behaviors in a Coastal Region: The Yukon River, Alaska and the Bering Sea

Kazuhiisa A. Chikita ^{1,*}, Tomoyuki Wada ², Isao Kudo ³, Sei-Ichi Saitoh ¹ and Mitsuhiro Toratani ⁴¹ Arctic Research Center, Hokkaido University, Sapporo 0010021, Japan; ssaitoh@arc.hokudai.ac.jp² Earth System Science, Inc., Tokyo 1600022, Japan; wada-tomoyuki@ess-jpn.co.jp³ Faculty of Fisheries Sciences, Hokkaido University, Hakodate 0418611, Japan; ikudo@fish.hokudai.ac.jp⁴ Department of Optical and Imaging Science and Technology, Tokai University, Hiratsuka 2591292, Japan; tora@keyaki.cc.u-tokai.ac.jp

* Correspondence: chikita@sci.hokudai.ac.jp; Tel.: +81-11-706-2764

Abstract: In the Bering Sea around and off the Yukon River delta, surface sediment plumes are markedly formed by glacier-melt and rainfall sediment runoffs of the Yukon River, Alaska, in June–September. The discharge and sediment load time series of the Yukon River were obtained at the lowest gauging station of US Geological Survey in June 2006–September 2010. Meanwhile, by coastal observations on boat, it was found out that the river plume plunges at a boundary between turbid plume water and clean marine water at the Yukon River sediment load of more than ca. 2500 kg/s. Grain size analysis with changing salinity (‰) for the river sediment indicated that the suspended sediment becomes coarse at 2 to 5‰ by flocculation. Hence, the plume’s plunging probably occurred by the flocculation of the Yukon suspended sediment in the brackish zone upstream of the plunging boundary, where the differential settling from the flocculation is considered to have induced the turbid water intrusion into the bottom layer.

Keywords: Yukon River plume; river discharge; sediment load; flocculation; plunging; underflow



Citation: Chikita, K.A.; Wada, T.; Kudo, I.; Saitoh, S.-I.; Toratani, M. Effects of River Discharge and Sediment Load on Sediment Plume Behaviors in a Coastal Region: The Yukon River, Alaska and the Bering Sea. *Hydrology* **2021**, *8*, 45. <https://doi.org/10.3390/hydrology8010045>

Academic Editor:
Carmelina Costanzo

Received: 17 February 2021
Accepted: 9 March 2021
Published: 12 March 2021

Publisher’s Note: MDPI stays neutral with regard to jurisdictional claims in published maps and institutional affiliations.



Copyright: © 2021 by the authors. Licensee MDPI, Basel, Switzerland. This article is an open access article distributed under the terms and conditions of the Creative Commons Attribution (CC BY) license (<https://creativecommons.org/licenses/by/4.0/>).

1. Introduction

One of actions of river discharge and sediment load into the ocean includes the sedimentation by energy dispersal in the estuarine area and through subsequent formation and advection of sediment plume in coastal and offshore regions. The sedimentary processes are often accompanied by the flocculation of suspended sediment, which affects nutrient and organic matters’ cycles connected to the food chain or ecosystem in the ocean [1]. Behaviors of river-suspended sediment can also be controlled by how the river water mixes with ocean water under shearing, where the flocculation again plays the important role on slow or rapid deposition of nutrient and organisms [2]. Hetland and Hsu [3] proposed a conceptual model of sedimentation in the estuarine, near-field plume, and far-field plume associated with the flocculation. However, there are a few quantitative descriptions of the flocculation effect on sediment dispersion and deposition [2,4]. Meanwhile, dynamic behaviors of the whole river plumes, including buoyant jets or bulges of small scale, have been explored by field observations, satellite image analysis, and numerical simulations, for example, for Mackenzie River plumes [5], Yellow River sediment plumes [6,7], Pearl River plumes [8], Columbia River plumes [9], small-mouth Kelvin number plumes [10], and Amazon River plumes [11,12]. With respect to the ecosystem in coastal regions, there are some remote-sensing studies of river sediment plume dynamics from the spatio-temporal variations of suspended sediment concentration (SSC; mg/L) [13,14]. Dean et al. [15] pointed out that satellite image analyses can be utilized for studies of the Yukon River plume behaviors. By using the river discharge time series from 2002–2014, Pitarch et al. [16]

related satellite-derived SSC of the Tiber River plume to the magnitude of the river discharge. However, the correlation between the discharge and SSC is very low at $R = 0.5$, because there is a lack of continuous data of river sediment load such as those of the river discharge and investigations of sediment depositional processes offshore from the river mouth.

In this study, considering a response of suspended sediment to a salinity change, behaviors of a river sediment plume in a coastal region are investigated by using time series of daily mean river discharge and sediment load in 2006–2010, which are here exemplified by the Yukon River, Alaska, and the Bering Sea.

2. Study Area

Most of the Yukon River drainage basin (area, $8.55 \times 10^5 \text{ km}^2$) belongs to the sub-arctic region south of the Arctic Circle ($66^\circ 33' \text{ N}$) and is occupied by 74.8% forest with discontinuous permafrost and 1.1% glacierized area in Alaska Range, Wrangell Mts., St. Elias Mts., etc. [17–20]. There are three USGS (U.S. Geological Survey) gauging stations along the main channel of the Yukon River. Site PLS is the lowest gauging station at ca. 170 km upstream of sites ALK and site EMK, base villages for the coastal observations (Figure 1). The Yukon River delta is radially formed with branching the Yukon River channel into some smaller river channels. Site EMK is located at ca. 18 km upstream of the delta front. The eastern shelf region of the Bering Sea ($2.29 \times 10^6 \text{ km}^2$ in area) is 50–70 m deep on average. The region at a distance of less than 170 km off the delta front is very shallow at less than 30 m in depth, which is due to sedimentation from sediment load of the Yukon River and the surrounding rivers. Behaviors of the Yukon sediment plume and the consequent dispersion of the plume-suspended sediment are controlled by the northern movement of the “Alaskan Coastal Water” [15,21], which is connected to the bottom distribution of clay minerals on the Alaskan-Chukchi margin [22].

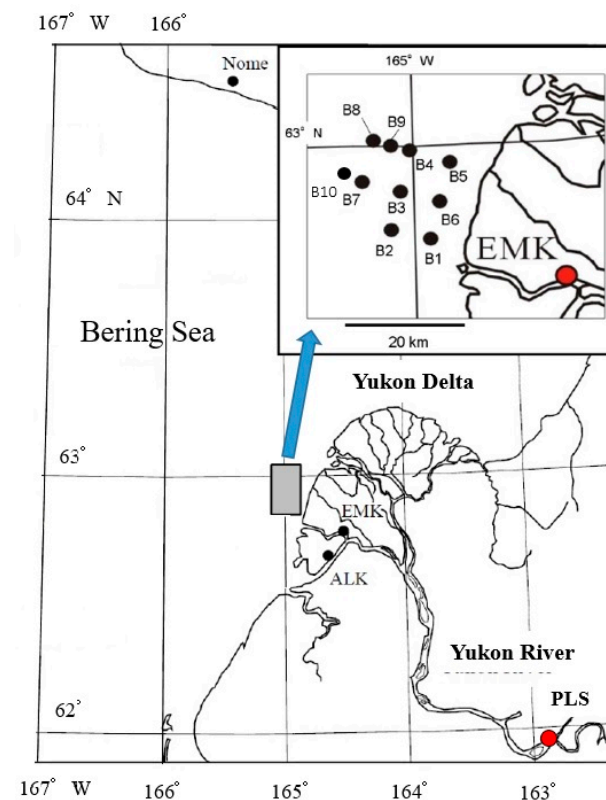


Figure 1. Location of ten observation sites off the Yukon delta front. The label “PLS” shows the location of the lowest USGS (U.S. Geological Survey) gauging station in the Yukon River.

With respect to the discharge and sediment load time series of the Yukon River, Chikita et al. [20] quantified the contribution of runoffs from the glacierized regions or the non-glacial regions to the total Yukon discharge and sediment load by the tank model, one of the runoff models. As a result, it was revealed that the contribution in the 1.1% glacierized area occupies 21.7–37.5%, and that most of the Yukon River suspended sediment originates from the glacial bedrock erosion in the glacierized regions and the resuspension in the river channels.

3. Methods

3.1. Field Observations

In order to obtain time series of suspended sediment load for the Yukon River, water turbidity was monitored at 1 h intervals at site PLS from June 2006–September 2010 by fixing a self-recording turbidimeter of infrared-ray back scattering type (model ATU3-8M, Alec Electronics, Inc.; range, 0–20,000 ppm; accuracy, $\pm 2\%$ of measured value) near the riverbank (Figure 1; Chikita et al. [19]). The turbidimeter had a wiper to keep the sensor window clean, which worked just before every hourly measurement. Thus, the dirt of the sensor window by organisms was prevented. Each of the hourly turbidity values was stored as an average of ten values measured instantaneously at 1 sec interval. The water turbidity (ppm) from the turbidimeter was converted into suspended sediment concentration (SSC: mg/L) by using the relationship between the turbidity, x , and the SSC, y , from the water sampled simultaneously at mid-channel ($y = 5.621x^{0.6762}$; $R^2 = 0.793$, $p < 0.01$) (Figure 2a). The regression curve is close to the one-to-one correspondence between turbidity and SSC. Water temperature was simultaneously measured every hour at site PLS by fixing a temperature logger, TidbiT v2 (Onset computer, Inc., Bourne, MA, USA; accuracy, ± 0.2 °C), to the turbidimeter. In order to know the representativeness of SSC and water temperature by the one-point method, during their monitoring, fluctuations of SSC and water temperature across the river channel were assessed by lowering a TTD (turbidity-temperature-depth) profiler from a boat [23]. As a result, differences between recorded SSC and water temperature and cross-sectionally averaged SSC and water temperature were less than 50 mg/L and less than 0.2 °C, respectively, being independent of their magnitude. The small differences between the two SSCs and the two water temperatures are due to the slow settling of suspended sediment (more than 90% silt and clay) and the complete turbulence of riverflow, respectively. Daily mean discharge data at site PLS were downloaded from the National Water Information System on the USGS web site (URL: http://waterdata.usgs.gov/nwis/dv/?site_no=15565447&agency_cd=USGS&referred_module=sw (accessed on 11 February 2021)). The sediment load, L (kg/s), was calculated by multiplying SSC, C (g/L in this calculation), by discharge, Q (m^3/s). The electric conductivity at 25 °C (EC25) and salinity of the Yukon River water were also obtained at site PLS using a portable EC meter (Type CM-14P, TOA Corporation; accuracy, ± 0.1 mS/m) for sampled water.

A relation between turbidity, x , and SSC, y , was obtained also for the sediment plume off the delta front. The regression curve was given by $y = 1.597x^{0.8119}$ ($R^2 = 0.932$, $p < 0.01$; Figure 2b), indicating that, in the region of brackish to oceanic waters, SSC is ca. 30% smaller than turbidity. This is probably due to an optical feature of marine water different from that of river water.

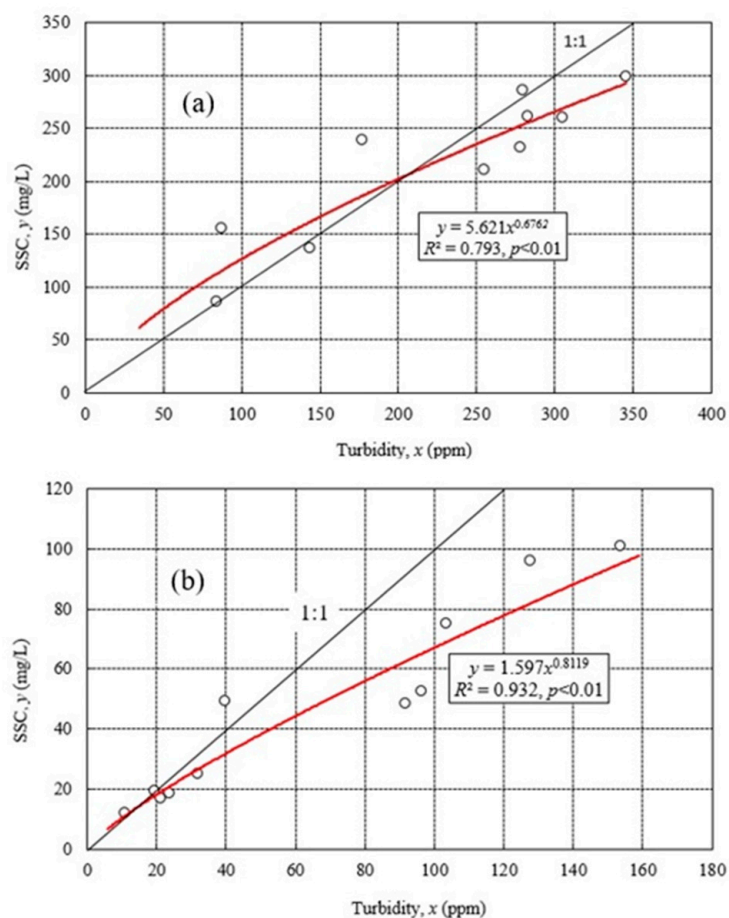


Figure 2. Relations between turbidity (ppm) and SSC (suspended sediment concentration; mg/L) at (a) site PLS and (b) the coastal region off the Yukon delta front.

At sites B1 to B10 in Figure 1, which were located at less than 30 km from the delta front near site EMK, profiler observations and water and sediment samplings were performed by boat on 6 September 2009 and 22 June 2010. A TCTD (turbidity-conductivity-temperature-depth) profiler (model ASTD687, JFE Advantech, Co., Ltd., Japan) was then utilized for the vertical measurements at 0.1 m pitch. The B5–B8 line and B6–B10 line correspond to two longitudinal lines offshore from the fan-shaped Yukon River delta.

With respect to the offshore extent of the Yukon sediment plume, relatively clear RGB (Red-Green-Blue color model) composite images of MODIS/aqua were downloaded from the NASA oceanic web site (URL: <https://oceancolor.gsfc.nasa.gov> (accessed on 19 and 24 February 2021)), which were selected on dates closest to those of the coastal observations.

3.2. Laboratory Experiments

During the turbidity record, river-suspended sediment and river-channel sediment were sampled at site PLS, and their grain size analyses were conducted by the photo-extinction method with a centrifuge for particles of grain size $d \leq 44 \mu\text{m}$ (micrometers) and by the sieving method for $d > 44 \mu\text{m}$ particles [19]. The channel sediment was a new one deposited in the glacier-melt and rainfall season of the year. With respect to the flocculation of river-suspended sediment in the coastal region, an effect of salinity on grain size of sediment was explored by suspending the river channel sediment in pure water of 0‰ and NaCl water of 2–35‰. In the grain size analyses, a sediment sample of $d \leq 44 \mu\text{m}$ in a quartz cell was repeatedly used with increasing the salinity from 0 to 35‰. Also, in order to know the existence of cohesive sediment such as kaolinite, illite, etc., clay particles of $d \leq 4 \mu\text{m}$ in river-suspended and plume-suspended sediments were mineralogically

identified by the X-ray diffraction (XRD) method. In the XRD method, a peak at a certain 2θ value (θ : Bragg angle) indicates the existence of one to three minerals specified.

4. Results

4.1. Time Series of Discharge and Sediment Load

Figure 3 shows temporal variations of (a) daily mean water temperature and SSC, and (b) discharge and sediment load at site PLS June 2006–September 2009. In late May or early June, the first large peaks of SSC, discharge, and sediment load in the year were produced by snowmelt runoffs just after the breakup of river ice. Then, water temperature greatly increased at more than $0\text{ }^{\circ}\text{C}$. Thereafter, glacier-melt and rainfall runoffs resulted in some peaks of SSC and sediment load in July–September. When glacier-melt sediment runoffs prevailed in July–August, water temperature decreased by $1\text{--}2\text{ }^{\circ}\text{C}$ after the peak in mid-July. In Figure 3b, it is seen that the sediment load at more than 3000 kg/s occurs for more 1 month as a whole. The water temperature was recorded at less than $0\text{ }^{\circ}\text{C}$ for a while in the ice-covered season. This means that the temperature logger was then enclosed by river ice, due to the ice growth.

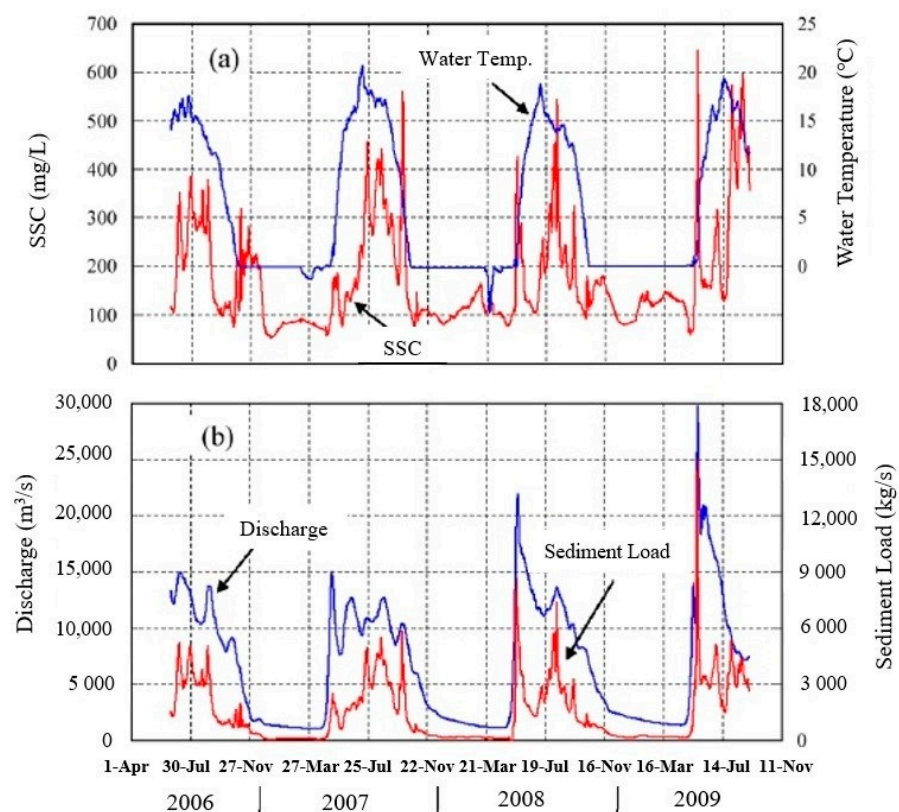


Figure 3. Temporal variations of (a) daily mean water temperature and SSC, and (b) daily mean discharge and sediment load at site PLS in June 2006–September 2009 (modified after Chikita et al. [19]).

4.2. Observational Results of Plume Behaviors

Figure 4 shows cross-sections of SSC, water temperature, salinity, and water density σ_T from the profiler observations on sites B5 to B8 line obtained on 6 September 2009 (Figure 1). Here, water density σ_T was calculated by $\sigma_T = \rho(S, T, 0) - 1000$, where $\rho(S, T, P)$ is water density (kg/m^3) and a function of salinity S (‰), water temperature T ($^{\circ}\text{C}$), and pressure P ($= 0$ at 1 atm). Here, the lag time of 2 days (equal to the distance, 170 km, divided by rough riverflow speed, 1 m/s) was considered as an approximate time needed to flow downstream from site PLS to the coastal region. The correspondent, daily mean SSC, discharge, sediment load, and water temperature at site PLS were 391 mg/L , $7.39 \times 10^3\text{ m}^3/\text{s}$, $2.89 \times 10^3\text{ kg/s}$, and $11.7\text{ }^{\circ}\text{C}$ on 4 September 2009, respectively.

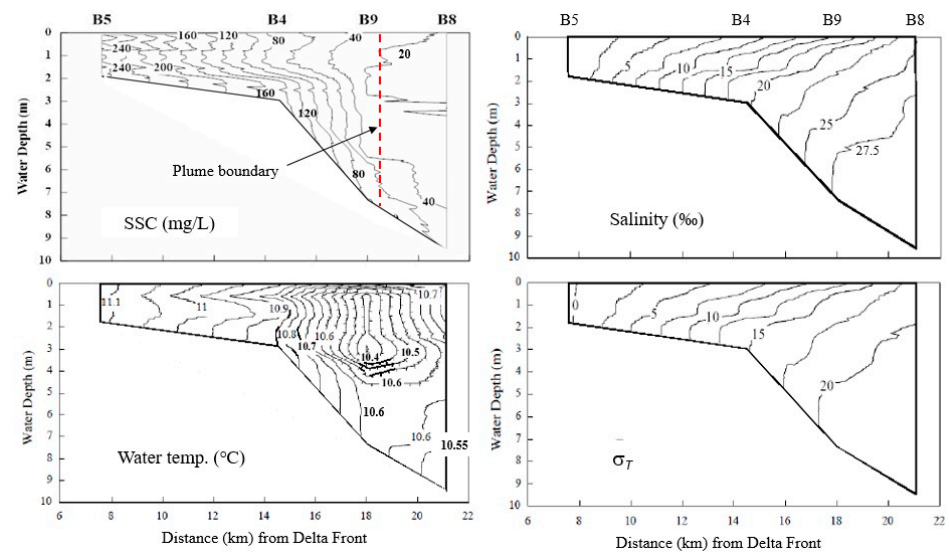


Figure 4. Longitudinal cross-sections of SSC, water temperature, salinity, and water density σ_T by the coastal observation on the B5–B8 line on 6 September 2009 (Figure 1). The dotted line in the SSC cross-section shows a boundary between turbid plume water and relatively clean ocean water observed in situ.

A boundary between the plume water and relatively clean marine water was clearly seen near site B9 as shown by the dotted vertical line in Figure 4. The SSC on the boundary, corresponding to a plunging point, was ca. 30 mg/L. Offshore from the boundary, a bottom layer at 40 mg/L or more SSC was observed probably as a downslope bottom current or underflow. This plunging seems to have been preceded on the gentle slope between sites B5 and B4, since the turbid water at SSC of 160–240 mg/L was accumulated near the bottom as a nepheloid layer. The water temperature distribution indicates that vertical mixing due to the entrainment occurred at the plunging point [24–26]. A boundary between the plume and marine water and the correspondent plunging were also observed between site B3 and site B7 (Figure 5). However, the resultant bottom current appears to have been advanced wholly in the lower layer of more than 27.5‰ salinity, since the SSC cross-section indicates a gradual SSC decrease offshore, accompanied by the vertical uniformity.

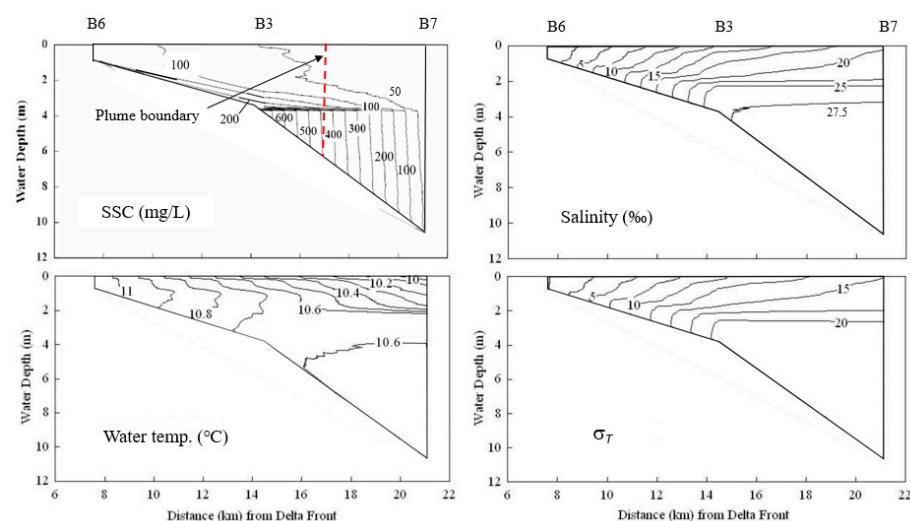


Figure 5. Longitudinal cross-sections of SSC, water temperature, salinity, and water density σ_T by the coastal observation on the B6–B7 line on 6 September 2009 (Figure 1). The dotted line in the SSC cross-section shows a boundary between turbid plume water and relatively clean ocean water observed in situ.

The traverse cross-section along the B1–B5 line (Figure 6) indicates that there is a zone with relatively high SSC of 140–250 mg/L between sites B6 and B5. This zone corresponds to the mixing zone upstream of the plunging points in Figures 4 and 5 [24], which is here accompanied by the vertical uniformity of SSC, water temperature, and salinity. Then, the SSC and water temperature decrease and the salinity increases gradually toward site B6 from site B5. This reflects the vertical mixing by relatively high river water flux at site B5. The longitudinal center of the sediment plume is, thus, located near site B5 rather than site B6 (Figure 1). If the high SSC zone on the B5–B6 line was produced by the resuspension of bottom sediment by tidal currents, wind-driven current, or littoral currents, then a high SSC zone should appear in the relatively shallow B6–B1 zone. Hence, the plunging is considered to have been raised through the mixing responding to the magnitude of the Yukon River sediment load.

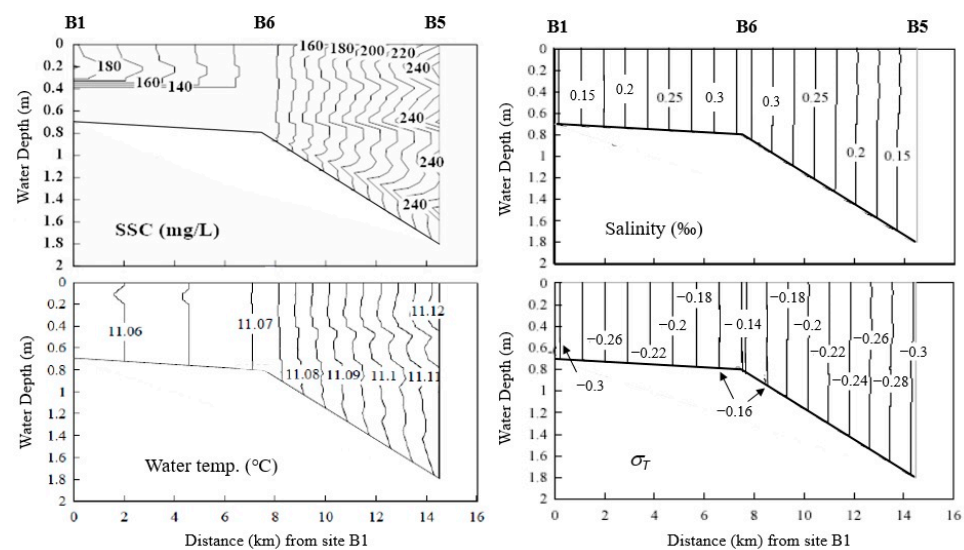


Figure 6. Traverse cross-sections of SSC, water temperature, salinity, and marine water density σ_T by the coastal observation on the B1–B5 line on 6 September 2009 (Figure 1).

Figure 7 shows longitudinal cross-sections of SSC, water temperature, salinity, and σ_T along the B6–B10 line by the coastal observation on 22 June 2010. The daily mean SSC discharge, sediment load, and water temperature at site PLS were 240 mg/L, $9.12 \times 10^3 \text{ m}^3/\text{s}$, $2.19 \times 10^3 \text{ kg/s}$, and $14.6 \text{ }^\circ\text{C}$ on 20 June 2010, respectively. The discharge was 19% larger than that on 4 September 2009, but sediment load was 24% smaller because SSC was 39% smaller than that on 4 September 2009. Then, a boundary between the plume and marine water was not clearly seen near site B3 or farther. Such a sediment plume’s plunging as in Figures 4 and 5 is, thus, judged not to have occurred. In fact, the SSC in the cross-section was relatively very small at 10–60 mg/L. The SSC was then vertically uniform, being probably due to turbulent mixing by relatively strong river-induced current from the higher river discharge.

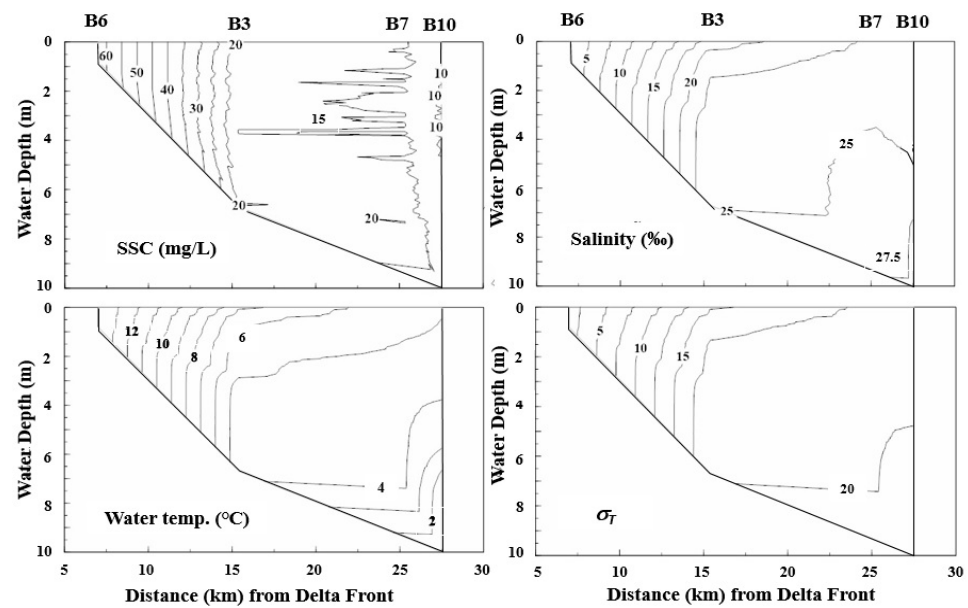


Figure 7. Longitudinal cross-sections of SSC, water temperature, salinity, and σ_T on the B6–B10 line by the coastal observation on 22 June 2010 (Figure 1).

4.3. Experimental Results for Yukon Sediment

Figure 8 shows a salinity effect on (a) cumulative grain size distributions of the Yukon channel sediment and (b) their mean size and standard deviation. When the salinity increased from 2 to 5‰, the suspended sediment became coarse at grain size $d < 16.5 \mu\text{m}$ with increasing the mean size from 16.6 to 19.0 μm . This means that the differential settling from flocculation or coagulation occurred at more than 2‰ salinity for the Yukon suspended sediment of $d < 16.5 \mu\text{m}$ [27]. At salinity of 10‰ or more, the grain size did not change greatly with mean size of 17.9 to 18.7 μm . The standard deviation decreased from 13.6 μm at 0‰ to 12.0 μm at 2‰, and then varied at a small range of 10.8 to 12.5 μm at 2–35‰. Hence, the addition of salinity to the suspension tends to increase the uniformity in grain size of suspended sediment, reflecting the flocculation. This experiment dealt with the behaviors of suspended sediment in still water. If a certain shearing by a flow was given, the flocculation could be more enhanced [28].

Figure 9 shows the mineralogy of Yukon River and plume suspended sediments at less than 4 μm in grain size by the XRD method. Such clay minerals as kaolinite, chlorite, smectite, and illite could easily produce the flocculation of suspended sediment in the brackish region offshore from the Yukon River mouth. The flocculation of clay particles induces the coarseness of the river-suspended sediment, which more rapidly accumulates the sediment near the bottom as an agent for the plunging. In fact, the plume-suspended sediment includes few clay minerals, suggesting their gravitational settling or deposition offshore from the delta front. Especially, kaolinite, smectite, and illite are more cohesive to easily flocculate.

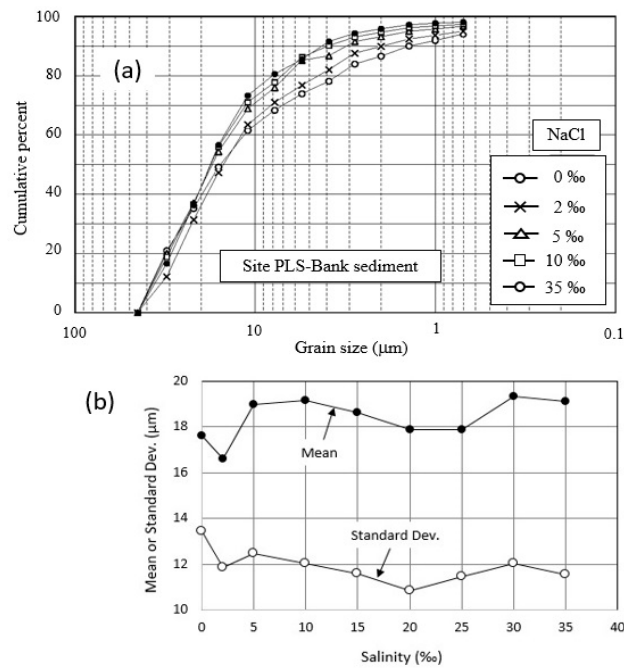


Figure 8. Changes in (a) cumulative grain size distributions and (b) correspondent mean size and standard deviation of the Yukon River bank sediment at grain size $d \leq 44 \mu\text{m}$ by increasing the salinity from 0 to 35 ‰.

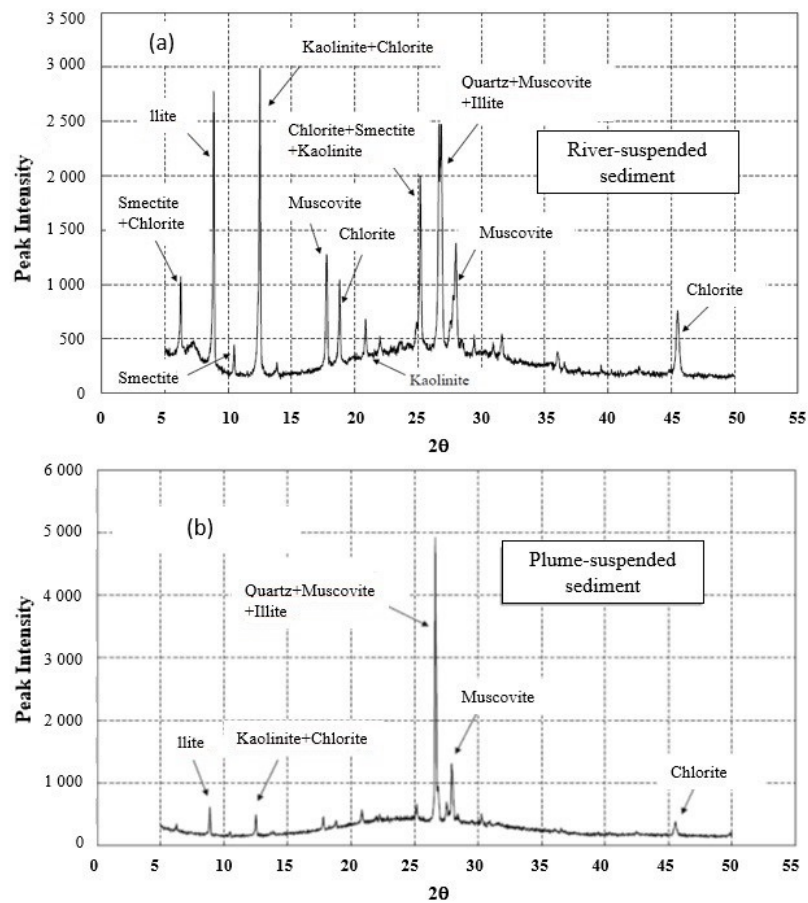


Figure 9. Mineralogy of suspended sediment at grain size $d \leq 4 \mu\text{m}$ by the X-ray diffraction method. The sediments were sampled at (a) site PLS and (b) site B9 in September 2009. θ : Bragg angle ($^\circ$).

5. Discussion

River-induced plumes released from a river mouth are dynamically dispersed by littoral, tidal, and wind-driven currents, and thereby control the ecosystem and sedimentation in coastal and offshore regions. However, the observational results in Figures 4–7 indicate that, in the estuarine and near-field plume regions, the magnitude of river discharge and sediment load could control the level of mixing between river water and ocean water and the subsequent dynamic behaviors of river-induced plume. The Yukon River has only water density $\sigma_T = -0.133$ at SSC of 391 mg/L, water temperature of 11.7 °C, and EC25 of 27 mS/m (salinity, 0.127‰) at site PLS on 4 September 2009. Thus, the plunging into the lower ocean water as in Figures 4 and 5 cannot occur under pycnal condition between the river water and ocean water. Otherwise, the differential settling from the flocculation of suspended sediment probably produced the nepheloid layer near the bottom in the mixing zone, followed by the underflow. The flocculation shown in Figure 8 could be enhanced by the shearing in the mixing zone and the existence of cohesive clay minerals such as kaolinite, smectite, and illite (Figure 9).

The plunging and subsequent underflow in Figures 4 and 5 appear to have been produced on the gentle slope between sites B5 and B4 or sites B6 and B3. By the comparison between Figures 4 and 6, it is seen that the plunging may occur at the Yukon River sediment load of more than ca. 2500 kg/s at site PLS. The sediment load of more than 2500 kg/s can be recorded in July–September (Figure 3), when the suspended sediment contains more fine-grained particles supplied by the glacier-melt and rainfall runoffs [20].

A two-dimensional hydrodynamic condition of the underflow in Figure 4 is judged by using the densimetric Froude number F_d and Reynolds number Re in the following:

$$F_d = U/(g'H_p)^{1/2}, \quad (1)$$

$$Re = UH_p/\nu, \quad (2)$$

where U is the underflow's velocity (m/s), H_p is the water depth (m) at the plunging point, $g' = g(\rho - \rho_0)/\rho_0$ (g : acceleration due to gravity in m/s^2 , ρ : underflow's density in kg/m^3 , ρ_0 : ambient water density in kg/m^3), and ν is the kinematic viscosity (m^2/s). From the σ_T distribution in Figure 4, $\rho = 1025 \text{ kg/m}^3$, $\rho_0 = 1020 \text{ kg/m}^3$, $H_p = 7.5 \text{ m}$, and $\nu = 1.32 \times 10^{-6} \text{ m}^2/s$ for salinity at 25‰ and water temperature at 10.6 °C gave $F_d = 0.017\text{--}0.17$ and $Re = 5.7 \times 10^4\text{--}5.7 \times 10^5$ in Equations (1) and (2). Then, $U = 0.01\text{--}0.1 \text{ m/s}$.

Similarly, for the underflow downstream of the plume boundary in Figure 5, $\rho = 1022 \text{ kg/m}^3$, $\rho_0 = 1015 \text{ kg/m}^3$, $H_p = 4.5 \text{ m}$, and $\nu = 1.33 \times 10^{-6} \text{ m}^2/s$ for 27‰ salinity and 10.6 °C water temperature, which gave $F_d = 0.018\text{--}0.18$ and $Re = 3.4 \times 10^4\text{--}3.4 \times 10^5$ at $U = 0.01\text{--}0.1 \text{ m/s}$. Thus, the underflow may be subcritical and turbulent, indicating the low entrainment from the ambient water above. This indicates that, in spite of the small scale, the underflow could flow down in a relatively long travel distance.

When the river discharge increased and the sediment load decreased, the mixing zone was extended offshore as in Figure 7, where the plunging was not observed. As far as seeing the RGB satellite images of the Yukon sediment plume (Figure 10) on the dates closest to those of the coastal observations, the extent of the surface plume appears to be much larger on 4 September 2009.

The Yukon River surface plume could be wholly advected northwestward by the "Alaskan Coastal Water" [21] (Figure 10). In Figures 4 and 5, there was no turbid surface layer in the location of the plunging and subsequent underflow formation. Thus, the liftoff of the sediment plume into the surface layer is considered to have occurred in more northeastern regions, where the surface sediment plume is extended northward (Figure 10a).

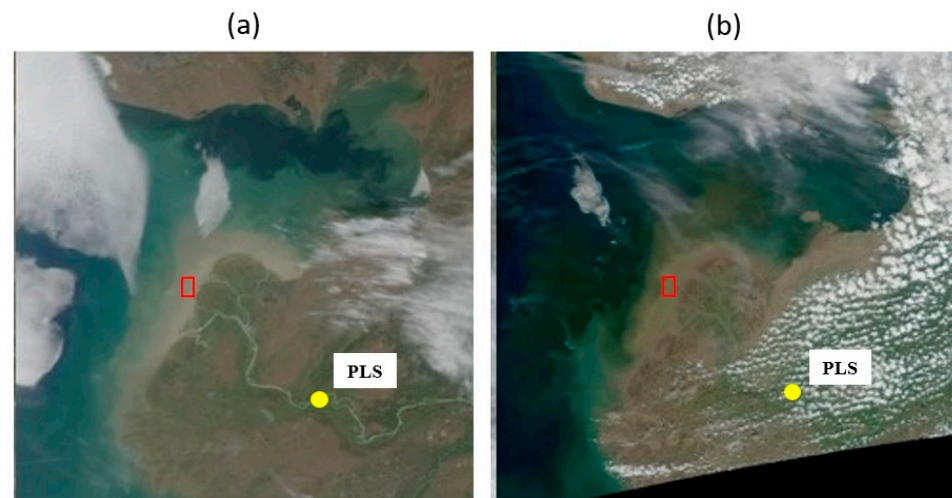


Figure 10. RGB (Red-Green-Blue color model) composite images of MODIS/Aqua on (a) 4 September 2009 and (b) 22 June 2010. The red rectangles show the area of the coastal observations on 6 September 2009 and 22 June 2010. The label “PLS” shows the location of the USGS gauging station at the Pilot Station village.

6. Conclusions

By the observations of Yukon River sediment plumes in the coastal region of the Bering Sea, it was found out that, at Yukon River sediment load of more than ca. 2500 kg/s, the plume plunges at a boundary of the plume and ocean water. The production of the bottom current or underflow from the plunging is probably due to the differential settling from the flocculation of river-suspended sediment. Both the suspended sediment concentration (SSC) and sediment load of the Yukon River were relatively high in the glacier-melt and rainfall runoffs of July–September. In such runoffs, suspended sediment becomes relatively fine, including clay minerals such as kaolinite, smectite, chlorite, and illite to easily make flocs in the brackish zone. Hence, temporal variations of glacier-melt and rainfall sediment runoffs of the Yukon River could change behaviors of the sediment plume in the coastal region. It was experimentally demonstrated that the flocculation of suspended sediment occurs at 2‰ or more salinity. This flocculation may produce the underflow in the deeper zone by accumulating the flocculated sediment on the onshore gentle slope. It should be needed to experimentally and theoretically clarify the mechanism of the underflow’s production from the flocculation.

Author Contributions: K.A.C., T.W. and I.K. participated in all the filed surveys to set and manage field instruments; K.A.C. wrote the paper; S.-I.S. conceived and designed the Yukon River—Bering Sea research project; M.T. analyzed many images of MODIS/Aqua. All authors have read and agreed to the published version of the manuscript.

Funding: This study was financially supported by the Japan Aerospace Exploration Agency (JAXA) as a research in the joint project of IARC/JAXA.

Acknowledgments: We appreciate the official support of Emeritus S. Akasofu, L. Hinzman and Y. Kim, the International Arctic Research Center (IARC), the University of Alaska at Fairbanks (UAF) and the welcome data supply of the U.S. Geological Survey.

Conflicts of Interest: The authors declare no conflict of interest.

References

1. Milligan, T.G.; Hill, P.S.; Law, B.A. Flocculation and the loss of sediment from the Po River plume. *Cont. Shelf Res.* **2007**, *27*, 309–321. [[CrossRef](#)]
2. Strom, K.; Keyvani, A. Flocculation in a decaying shear field and its implications for mud removal in near-field river mouth discharges. *J. Geophys. Res. Oceans* **2016**, *121*, 2142–2162. [[CrossRef](#)]

3. Hetland, R.; Hsu, T. Freshwater and sediment dispersal in large river plumes. In *Biogeochemical Dynamics at Major River-Coastal Interfaces: Linkages with Global Change*; Bianchi, T., Allison, M., Cai, W., Eds.; Cambridge University Press: Cambridge, UK, 2013; pp. 55–85. [\[CrossRef\]](#)
4. Markussen, T.N.; Elberling, B.; Winter, C.; Andersen, T.J. Flocculated meltwater particles control Arctic land-sea fluxes of labile iron. *Sci. Rep.* **2016**, *6*, 24033. [\[CrossRef\]](#) [\[PubMed\]](#)
5. Milligan, R.P.; Perrie, W.; Solomon, S. Dynamics of the Mackenzie River plume on the inner Beaufort shelf during an open water period in summer. *Estuar. Coast. Shelf Sci.* **2010**, *89*, 214–220. [\[CrossRef\]](#)
6. Qiao, S.; Shi, X.; Zhu, A.; Liu, Y.; Bi, N.; Fang, X.; Yang, G. Distribution and transport of suspended sediments off the Yellow River (Huanghe) mouth and the nearby Bohai Sea. *Estuar. Coast. Shelf Sci.* **2010**, *86*, 337–344. [\[CrossRef\]](#)
7. Wang, H.; Bi, N.; Wang, Y.; Saito, Y.; Yang, Z. Tide-modulated hyperpycnal flows off the Huanghe (Yellow River) mouth, China. *Earth Surf. Process. Landf.* **2010**, *35*, 1315–1329. [\[CrossRef\]](#)
8. Pan, J.; Gu, Y.; Wang, D. Observations and numerical modeling of the Pearl River plume in summer season. *J. Geophys. Res. Oceans* **2014**, *119*, 2480–2500. [\[CrossRef\]](#)
9. Saldias, G.; Shearman, R.K.; Barth, J.A.; Tuffiaro, N. Optics of the offshore Columbia River plume from glider observations and satellite imagery. *J. Geophys. Res. Oceans* **2016**, *121*, 2367–2384. [\[CrossRef\]](#)
10. Cole, K.L.; Hetland, R.D. The effects of rotation and river discharge on net mixing in small-mouth Kelvin number plumes. *J. Phys. Oceanogr.* **2016**, *46*, 1421–1436. [\[CrossRef\]](#)
11. Varona, H.L.; Veleda, D.; Silva, M.; Cintra, M.; Araujo, M. Amazon River plume influence on Western Tropical Atlantic dynamic variability. *Dyn. Atmos. Oceans* **2019**, *85*, 1–15. [\[CrossRef\]](#)
12. Gouveia, N.A.; Gherardi, D.F.M.; Aragão, L.E.O.C. The role of the Amazon River plume on the intensification of the hydrological cycle. *Geophys. Res. Lett.* **2019**, *46*, 12221–12229. [\[CrossRef\]](#)
13. de Oliveira, E.N.; Knoppers, B.A.; Lorenzetti, J.A.; Medeiros, P.R.P.; Carneiro, M.E.; de Souza, W.F.L. A satellite view of riverine turbidity plumes on the NE-E Brazilian coastal zone. *Braz. J. Oceanogr.* **2012**, *60*, 283–298. [\[CrossRef\]](#)
14. Restrepo, J.D.; Park, E.; Aquino, S.; Latrubesse, E.M. Coral reefs chronically exposed to river sediment plumes in the southwestern Caribbean: Rosario Islands, Colombia. *Sci. Total Environ.* **2016**, *553*, 316–329. [\[CrossRef\]](#)
15. Dean, K.G.; McRoy, C.P.; Ahlnäs, K.; Springer, A. The plume of the Yukon River in relation to the Oceanography of the Bering Sea. *Remote Sens. Environ.* **1989**, *28*, 75–84. [\[CrossRef\]](#)
16. Pitarch, J.; Falcini, F.; Nardin, W.; Brando, V.E.; Di Cicco, A.; Marullo, S. Linking flow-stream variability to grain size distribution of suspended sediment from a satellite-based analysis of the Tiber River plume (Tyrrhenian Sea). *Sci. Rep.* **2016**, *9*, 19729. [\[CrossRef\]](#)
17. Brabets, T.P.; Wang, B.; Meade, R.H. *Environmental and Hydrologic Overview of the Yukon River Basin, Alaska and Canada*; Water-Resources Investigations Report; U. S. Geological Survey: Anchorage, AK, USA, 2000. [\[CrossRef\]](#)
18. Striegl, R.G.; Dornblaser, M.M.; Aiken, G.R.; Wickland, K.P.; Raymond, P.A. Carbon export and cycling by the Yukon, Tanana, and Porcupine Rivers, Alaska, 2001–2005. *Water Resour. Res.* **2007**, *43*, W02411. [\[CrossRef\]](#)
19. Chikita, K.A.; Wada, T.; Kudo, I.; Kim, Y. The intra-annual variability of discharge, sediment load and chemical flux from the monitoring: The Yukon River, Alaska. *J. Water Resour. Prot.* **2012**, *4*, 173–179. [\[CrossRef\]](#)
20. Chikita, K.A.; Wada, T.; Kudo, I. Material-loading processes in the Yukon River basin, Alaska: Observations and modelling. *Low Temp. Sci.* **2016**, *74*, 43–54. [\[CrossRef\]](#)
21. Nelson, H.; Creager, J.S. Displacement of Yukon-derived sediment from Bering Sea to Chukchi Sea during Holocene time. *Geology* **1977**, *5*, 141–146. [\[CrossRef\]](#)
22. Ortiz, J.D.; Polyak, L.; Grebmeier, J.M.; Darby, D.; Eberl, D.D.; Naidu, S.; Nof, D. Provenance of Holocene sediment on the Chukchi-Alaskan margin based on combined diffuse spectral reflectance and quantitative X-ray diffraction analysis. *Glob. Planet. Chang.* **2009**, *68*, 73–84. [\[CrossRef\]](#)
23. Chikita, K.A.; Kemnitz, R.; Kumai, R. Characteristics of sediment discharge in the subarctic Yukon River, Alaska. *Catena* **2002**, *48*, 235–253. [\[CrossRef\]](#)
24. Chikita, K. A field study on turbidity current initiated from spring runoffs. *Water Resour. Res.* **1989**, *25*, 257–271. [\[CrossRef\]](#)
25. Chikita, K. Sedimentation by river-induced turbidity currents: Field measurements and interpretation. *Sedimentology* **1990**, *37*, 891–905. [\[CrossRef\]](#)
26. Knoblach, H. *Overview of Density Flows and Turbidity Currents*; Water Resources Research Laboratory, U.S. Bureau of Reclamation: Denver, CO, USA, 1999; pp. 1–27.
27. Whitehouse, U.G.; James, L.M.; Debbrecht, J.D. Differential settling tendencies of clay minerals in saline waters. *Clays Clay Miner.* **1958**, *7*, 1–79. [\[CrossRef\]](#)
28. Lick, W.; Huang, H.; Jepsen, R. Flocculation of fine-grained sediments due to differential settling. *J. Geophys. Res. Oceans* **1993**, *98*, 10279–10288. [\[CrossRef\]](#)